Selected Technical Papers
ASTM INTERNATIONAL

# On High Fluence Irradiation Hardening of Nine RPV Surveillance Steels in the UCSB ATR-2 Experiment: Implications to Extended Life Embrittlment Predictions

| | |
|---|---|
| Journal: | *STP: Selected Technical Papers* |
| Manuscript ID | Draft |
| Manuscript Type: | Full Length Paper |
| Date Submitted by the Author: | n/a |
| Complete List of Authors: | Nanstad, Randy; R&S consultants, LLC, ; Oak ridge National Laboratory, Materials Science and Techology Division<br>Almirall, Nathan; University of California Santa Barbara<br>Server, William; ATI Consulting,<br>Wells, Peter; University of California Santa Barbara<br>Sokolov, Mikhail; Oak Ridge National Laboratory, Materials Science and Technology<br>Long, Elliot; EPRI,<br>Odette, G. Robert; University of California Santa Barbara |
| ASTM Committees and Subcommittees: | E10.02 Behavior and Use of Nuclear Structural Materials < E10 Committee on Nuclear Technology and Applications |
| Keywords: | Radiation embrittlement, flux effects, microhardness, shear punch, transition temperature shift correlations, high fluence data |
| Abstract: | Nine archival reactor pressure vessel (RPV) surveillance steels from commercial nuclear power plants were irradiated in the UCSB Advanced Test Reactor 2 (ATR-2) experiment to evaluate irradiation embrittlement under low flux surveillance capsule versus higher flux test reactor (ATR-2) conditions. The post-irradiation measurements of irradiation hardening, measured as increases in yield stress ($\Delta\sigma_y$), and corresponding conversions of $\Delta\sigma_y$ to Charpy V-notch 41 J transition temperature shifts ($\Delta T_c$), are compared to various embrittlement trend curve (ETC) model predictions for the nine steels. Tensile, and converted shear punch and microhardness measurements of $\Delta\sigma_y$ generally show a continuing increase between intermediate and the high ATR-2 fluences. The EONY and E900 ETC models underpredict embrittlment at the ATR-2 irradiation condition of: irradiation temperature ($T_i$) of 292°C, neutron fluence ($\Phi t$) of $1.4x10^{20}$ n/cm$^2$ (E > 1 MeV) and neutron flux ($\Phi$) of $3.68x10^{12}$ n/cm$^2$-s. On average, the French FIS and Japanesea JAEC ETCs slightly overpredict the ATR-2 data. The increase in $\Delta\sigma_y$ with higher fluence is primarily due to Ni-Mn-Si precipitates, which slowly evolve in both nearly copper free and copper bearing steels. Finally, a new OWAY embrittlement model is shown which yields good predictions for the 9 steels at high fluences ($\Phi t > 5.5x10^{19}$ n/cm$^2$). |

# On High Fluence Irradiation Hardening of Nine RPV Surveillance Steels in the UCSB ATR-2 Experiment: Implications to Extended Life Embrittlment Predictions

**Randy K. Nanstad[1], Nathan Almirall[2], Peter Wells[2], William L. Server[3] Mikhail A. Sokolov[1], Elliot J. Long[4] and G. Robert Odette[2]**

## Abstract

Nine archival reactor pressure vessel (RPV) surveillance steels from commercial nuclear power plants were irradiated in the UCSB Advanced Test Reactor 2 (ATR-2) experiment to evaluate irradiation embrittlement under low flux surveillance capsule versus higher flux test reactor (ATR-2) conditions. The post-irradiation measurements of irradiation hardening, measured as increases in yield stress ($\Delta\sigma_y$), and corresponding conversions of $\Delta\sigma_y$ to Charpy V-notch 41 J transition temperature shifts ($\Delta T_c$), are compared to various embrittlement trend curve (ETC) model predictions for the nine steels. Tensile, and converted shear punch and microhardness measurements of $\Delta\sigma_y$ generally show a continuing increase between intermediate and the high ATR-2 fluences. The EONY and E900 ETC models underpredict embrittlment at the ATR-2 irradiation condition of: irradiation temperature ($T_i$) of 292°C, neutron fluence ($\phi t$) of $1.4x10^{20}$ n/cm$^2$ (E > 1 MeV) and neutron flux ($\phi$) of $3.68x10^{12}$ n/cm$^2$-s. On average, the French FIS and Japanesea JAEC ETCs slightly overpredict the ATR-2 data. The increase in $\Delta\sigma_y$ with higher fluence is primarily due to Ni-Mn-Si precipitates, which slowly evolve in both nearly copper free and copper bearing steels. Finally, a new OWAY embrittlement model is shown which yields good predictions for the 9 steels at high fluences ($\phi t > 5.5x10^{19}$ n/cm$^2$).

## Key Words

Radiation embrittlement, flux effects, microhardness, shear punch, transition temperature shift correlations, high fluence data

[1]Oak Ridge National Laboratory; [2]University of Californias Santa Barbara; [3]ATI Consulting; [4]Electric Power Research Institute

## 1. Introduction

Reactor pressure vessel (RPV) integrity is the primary safety concern for light water nuclear reactors. At the start of life, the fracture toughness of RPV steels is sufficiently high so as to assure vessel integrity However, RPV steels close to the reactor core experience neutron irradiation embrittlement. The degree of embrittlement, manifested as the degradation of fracture toughness, with an attendant increase in yield stress ($\Delta\sigma_y$), depends on the sensitivity of a particular RPV steel [1,2].

Embrittlement is traditionally monitored by shifts in the transition temperature measured using shifts in Charpy V-notch energy-temperature curves ($\Delta T_c$) indexed at 41 J, as well as decreases in upper shelf energy. Many different predictive $\Delta T_c$ models, typically called embrittlement trend curves (ETCs), have been developed in different countries [3]. The ETCs are largely based on power reactor surveillance capsule data representing the fleet of reactors in each country. While these models are generally robust up to intermediate fluences, on the order of $5x10^{19}$ n/cm$^2$ (E > 1 MeV), extrapolations to higher, end of extended life fluences, nominally of order $10^{20}$ n/cm$^2$, are more uncertain, since there is relatively little surviallance data for these conditions. One way to supplement surviellance data at higher fluences is the use of accelerated test reactor irradiations. However, this approach naturally raises the issue of flux effects on embrittlement, known to be important at low fluence [2]. Note, embrittlement variables are highly interactive, and act in combination to mediate $\Delta T_c$. It is also well established that changes in the yield strength ($\Delta\sigma_y$) are related to $\Delta T_c$. Thus, it is critical to measure $\Delta T_c$, $\Delta\sigma_y$ and the underlying microstructural evolutions, over a wide range of fluxes, for a large matrix of alloys covering pertinent ranges of irradiation fluences and temperatures.

The results presented in this paper are based on high fluence data from a test reactor irradiation of nine RPV surveillance steels, which are compared to actual surveillance data for a range of lower fluxes and fluences [3]. Due to limitations in space in the test reactor irradiation, the $\Delta\sigma_y$ for the large steel matrix was characterized by tensile, microhardness, and shear punch tests. Results from the actual surveillance programs are based on Charpy V-notch and tensile tests. Thus, correlations between microhardness, shear punch and tensile test yield strength changes ($\Delta\sigma_y$), as well as between the $\Delta\sigma_y$ and Charpy V-notch $\Delta T_c$ were developed to allow intercomparisons of the surviellance and ATR-2 data.

Seven of the steels in the ATR-2 irradiation program described in this paper are currently being irradiated to high fluence in operating commercial Pressurized Water Reactors (PWRs) in an Electric Power Research Institute (EPRI) project called the PWR Supplemental Surveillance Program (PSSP) [5]. Thus, there will be an opportunity to assess the effect of neutron flux, as well as the property-property correlation procedures, for these steels. In the meantime, the high fluence test reactor data are compared with embrittlement trend predictions used in several countries, including the new Odette, Wells, Almirall, Yamamoto (OWAY) model [2].

## 2. ATR-2 Test Reactor Irradiation and Materials

Details on the irradiation conditions in the Idaho National Laboratory Advanced Test Reactor 2 (ATR-2) are described elsewhere, along with the overall test matrix [6-8]. Nine commercial RPV steels that have surveillance capsule results were irradiated to a fluence of ~ $1.38 \times 10^{20}$ n/cm$^2$ (E > 1 MeV) in the ATR test reactor at an average temperature of 292°C [6-8]. The chemical composition of the nine archival steels are listed in Table 1. The five elements, which are major embrittlement variables (Cu, Ni, Mn, Si, and P), highlighted in red bold numbers, cover a broad range of compostions: copper 0.03 to 0.36 wt%, nickel 0.19 to 0.95 wt%,

manganese 0.79 to 1.44 wt%, silicon 0.18 to 0.50 wt%, and phosphorous 0.004 to 0.016 wt%. The compositions were taken from the Reactor Embrittlement Archive Project (REAP) compilation of the data, developed at Oak Ridge National Laboratory for the U.S. Nuclear Regulatory Commission (USNRC), other information contained in commercial reactor vessel surveillance reports and the ASTM Plotter package [9,10]

Table 1. Compositions of the nine archival commercial reactor surveillance steels.

| Code | Material (Heat) | Cu | Ni | Mn | Si | P | Cr | Mo | C | S |
|---|---|---|---|---|---|---|---|---|---|---|
| A | Linde 91 weld (33A277) | **0.14** | **0.19** | **1.06** | **0.27** | **0.016** | 0.06 | 0.50 | 0.13 | 0.009 |
| B | SA533B-1 plate (C7466-1) | **0.20** | **0.60** | **1.33** | **0.23** | **0.005** | 0.11 | 0.49 | 0.22 | 0.016 |
| C | SA 508-2 forging (123X167VA1) | **0.06** | **0.75** | **0.79** | **0.28** | **0.010** | 0.35 | 0.58 | 0.20 | 0.009 |
| D | Linde 1092 weld-M (1P3571) | **0.36** | **0.78** | **1.42** | **0.18** | **0.013** | 0.04 | 0.49 | 0.18 | 0.011 |
| E | SA533B-1 plate (C0544-2) | **0.05** | **0.56** | **1.32** | **0.24** | **0.010** | 0.08 | 0.59 | 0.24 | 0.016 |
| F | Linde 1092 weld-K (1P3571) | **0.22** | **0.72** | **1.37** | **0.20** | **0.016** | 0.09 | 0.48 | 0.12 | 0.011 |
| G | SMAW (BOLA) | **0.03** | **0.90** | **0.94** | **0.32** | **0.004** | 0.03 | 0.23 | 0.14 | 0.014 |
| H | Linde 124 weld (4P4784)) | **0.04** | **0.95** | **1.41** | **0.45** | **0.009** | 0.13 | 0.48 | 0.09 | 0.009 |
| I | Linde 80 Weld, SA-1094 (71249 flux lot 8457) | **0.29** | **0.60** | **1.44** | **0.50** | **0.014** | 0.14 | 0.36 | 0.10 | 0.011 |

Subsized 16x4x0.5 mm SSJ-2 tensile and multi-purpose disc specimens were machined from the archival steels. Two to three tests of tensile specimens, with guage section of 5 or 2.2 mm, were carried out at the University of California, Santa Barbara (UCSB) using an MTS 810 load frame, in accordance with ASTM E8/E8M-16 [11], at a displacement rate of 0.008 mm/s resulting in strain rates in the range of 0.002 to 0.004/min. Standard engineering stress-strain, $\sigma(\varepsilon)$, curves were based on individual specimen thickness measurements, and a best fit to the elastic loading line was used to establish the 0.2% offset yield stress ($\sigma_y$). The ultimate engineering stress ($\sigma_u$) and uniform engineering strain at maximum load were also determined. The irradiated tests were generally stopped after maximum load to keep the specimens intact.

Both tensile specimen guage sections gave the same highly reproducable results with an overall standard deviation of in $\Delta\sigma_y$ and $\Delta\sigma_u$ of ~ 10 MPa.

Vickers microhardness ($H_v$) measurements were conducted at UCSB in accordance with ASTM E384-16 [12]. $H_v$ tests were also performed at ORNL in accordance with ASTM E92-16 [13]. At ORNL $H_v$ was taken as the average of 5 indents made using 10 kg loads on unpolished 20 mm and 8 mm diameter discs. At UCSB, $H_v$ was taken as the average of 10, or more, indents using 0.5 kg loads on polished 3 mm diameter discs, punched from the larger discs using an UCSB device designed maintain specimen flatness. The average diference between the ORNL and UCSB $H_v$ was less than 2%. The standard deviation in the hardness measurements was ~ 5 DPH ($kg/mm^2$), which corresponds to ~ 50 MPa.

Details of a shear punch test using the semiautomated apparatus developed at UCSB are described elsewhere [14]. Basically, a precision punch and die fixture blanked 3 mm discs from multipurpose coupons, while measuring the corresponding loads and displacements. The load-dislacements curves were converted to equivalent shear stresses ($\tau$) and strains ($\gamma$), as the steel deforms between the punch and die. The shear yield stress ($\tau_y$) was determined at a 1% offset from the elastic load line, while the maximum load defined $\tau_u$. The standard deviation in $\tau_y$ and $\tau_y$ was ~ 7 MPa.

Previous standard practice was to convert $\Delta H_v$ and $\Delta\tau_y$ to $\Delta\sigma_y$ using simple empirical correlations. However, it is more accurate to first evaluate the $\sigma_{yi}$ for the irradiated $H_{vi}$ and $\tau_{yi}$ to estimate the corresponding $\Delta\sigma_y$, by subtracting the unirradiated tensile test $\sigma_y$. The unirradiated tensile $\sigma_y$ data are generally available and more accurate than estimates based on the $H_v$ and SPT methods. The empirically observed relation $\sigma_y/\tau_y$ for the 9 unirradeted steels was found to be

identical to the ideal Von Mises of value of 1.73. However, the ratio increases in irradiated steels to an average of ~ 1.89. This difference is largely due to the reduction of strain hardening, since a significant zone of plastic shear deformation precedes the 1% offset for $\tau_y$. Notably, the $\sigma_y/\tau_y$ values for the 9 surveillance steels are close to those found in an analysis of a much larger ATR-2 database.

Likewise, it is necessary to convert the irradiated $H_v$ to $\sigma_y$. It has been shown that $H_v$ values contain an average flow stress ($\sigma_f$) contribution, between 0 and 10% plastic strain, associated with the indent [15]. This effect can be conceptually understood as the finite hardness which would be measured in a material with a $\sigma_y = 0$, due to finite strain hardening at the substantial indentation strains. Thus $H_v$ and $\sigma_y$ are approximately related as $\sigma_y - C_1 (< 0) + C_2H_v$. For commonly used units for $\sigma_y$ and $H_v$ of MPa and DPH (kg/mm$^2$), $C_1 = (\sigma_y - \sigma_f)$, which can be approximated as $C_1 \sim (\sigma_y - \sigma_u)$. The corresponding Vickers $C_2$ coefficient ($\sigma_y$-$H_v$ slope, MPa/DPH) is ~ 3 for elastic-perfectly plastic materials [16]. In practice, the $\sigma_y$-$H_v$ slope, $C_2$, can be established by fitting $\sigma_y$ versus $H_v$ data. Here, a fit to the unirradiated and irradiated data together was used in order to obtain a useful spread in $H_v$ and $\sigma_y$ data points. The $C_1$ intercept was ~ -94 MPa, which is remarkably close to the average $\sigma_u - \sigma_y$ for the combined unirradiated and irradiated data sets of 89 MPa. The corresponding $C_2$ slope is 2.8 MPa/DPH, which is 7% lower than the elastic-perfectly plastic value of 3.

The SPT and $H_v$ estimates of $\Delta\sigma_y$ derived from the irradiated $\tau_y$ and $H_v$ based $\sigma_{yi}$ minus the unirradiated tensile test $\sigma_{yu}$ are shown in Table 2 and Figure 1. While the SPT and $H_v$ based irradiated $\sigma_{yi}$ generally track each other, the corresponding $\Delta\sigma_y$ for the later are more accurate with a predicted minus measured standard devition of 22.7 MPa with a -1.1 average bias.

Table 2. Tensile, SPT and $H_v$ estimates of $\Delta\sigma_y$ (MPa).

| Steel | Tensile | ± | SPT | ± | Hv | ± |
|---|---|---|---|---|---|---|
| A | 165 | 19 | 123 | 22 | 142 | 16 |
| B | 244 | 7 | 258 | 9 | 253 | 17 |
| C | 118 | 17 | 161 | 49 | 146 | 21 |
| D | NA | NA | 315 | 35 | 259 | 13 |
| E | 151 | 18 | 149 | 20 | 152 | 32 |
| F | 291 | 19 | 310 | 46 | 308 | 23 |
| G | 144 | 19 | 180 | 6 | 154 | 13 |
| H | 206 | 12 | 206 | 10 | 165 | 12 |
| I | 271 | 11 | 231 | 33 | 260 | 13 |

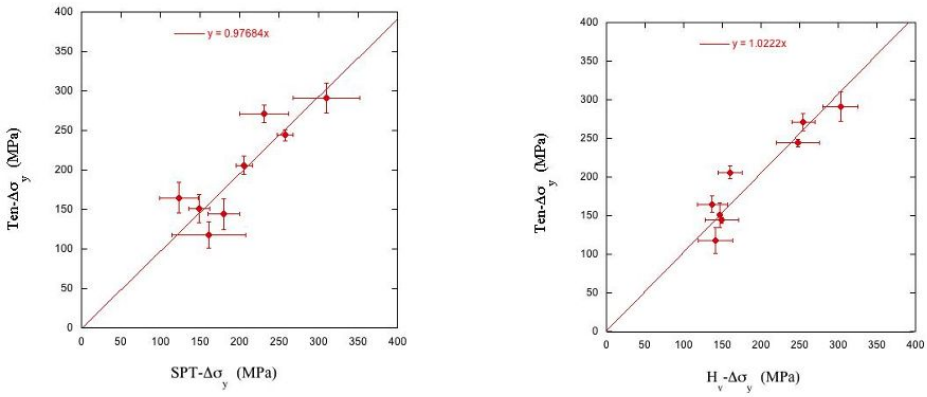


Figure 1. Tensile $\Delta\sigma_y$ versus estimates based on SPT (a) and $H_v$ (b) data.

It is useful to compare the measured ATR-2 test reactor irradiation results with the measured surveillance data for the same steels, even though the surveillance data are at lower fluences. The surveillance $\Delta\sigma_y$ and $\Delta T_c$ data were extracted from the USNRC REAP data base, some additional surveillance reports and the ASTME-10 PLOTTER package. All the $\Delta\sigma_y$ data are for room temperature. To make such comparisons the surveillance $\Delta T_c$ data must be converted to a equivalent $\Delta\sigma_y$, as $\Delta T_c = C_c\Delta\sigma_y$. A generic relation for $C_c(\Delta\sigma_y)$, derived from a large data base, has been used in the past [17-19]. In this case $C_c$ is a function of $\Delta\sigma_y$ and is

slightly different for plates and welds. However, the generic $C_c(\Delta\sigma_y)$ represents mean behavior.

It is well established that $C_c$ (at 41J) also varies with the initial unirradiated Charpy transition temperature and upper shelf energy, the upper shelf energy after irradiation and the coarse scale steel microstuctucture [17]. Thus, when possible, a better approach is to least square fit pairs of $\Delta\sigma_y$ - $\Delta T_c$ data for individual steels. The fit $C_c$ results for the 9 steels in this study are shown in Table 3 based on imposing 0,0 intercepts (note, allowing a finite intercept has little effect). Since the relative scatter for low levels of hardening data is large, Table 3 also shows the $C_c$ average of the $\Delta T_c/\Delta\sigma_y$ data for $\Delta\sigma_y > 50$ MPa. The two $C_c$ values are similar, except in one case where the larger value is probably more reliable.

Table 3. $C_c$ (= $\Delta T/\Delta\sigma_y$) based on measured pairs in the surveillance database for the 9 steels.

| Steel | Fitted | Average |
|---|---|---|
| A | 0.67 | 0.73 |
| B | 0.59 | 0.62 |
| C | 0.42 | 0.43 |
| D | 0.63 | 0.63 |
| E | 0.67 | 0.66 |
| F | 0.53 | 0.52 |
| G | 0.3 | 0.45 |
| H | 0.45 | 0.46 |
| I | 0.64 | 0.64 |

Figure 2a-i plot the actual measured $\Delta T_c$ as a function of fluence for the surveillance data (open squares) compared to the corresponding predicted $\Delta T_c$ based on the tensile test $\Delta\sigma_y$ (and in one case (D) the average of the SPT and $H_v$ converted $\Delta\sigma_y$) for both the individual steel $C_c$ estimates (blue triangle for the fitted and green diamond for the average $C_c$), as well as the

generic function (red circle). The generic $C_c$ based $\Delta T_c$ show large overpredictions in some cases, with a standard deviation and bias of 20 and 3.9, respectively. The agreement is much better for the averaged and fitted values. with a standard deviations of 12 MPa and biases of -2 and -0.3 MPa, respectively. Figure 2 also shows that the corresponding $\Delta\sigma_y$ based estimates of $\Delta T_c$ increases approximately linearly between surveillance and the higher ATR-2 fluence, with 2 exceptions. This behavior has been widely observed and is a key feature of the OWAY model as discussed in Section 4. Figure 3a-i show the direct comparison of measured and predicted $\Delta T_c$ for least square fitted, averaged, or based on the generic fit $C_c$'s.

## 3. Comparison of Estimated High Fluence Mechanical Properties with Current Embrittlement Trend Equations

A number of empirical, or semi-empirical, $\Delta T_c$ models have been proposed in different countries [1-3,18-25], in some cases motivated by the physics of embrittlement [2, 23]. Most of these so-called embrittlement trend curves (ETC) are based on correlations of country-specific surveillance capsule databases. The ETC generally account for Ni, Cu, P and other elements, product form, fluence, irradiation temperature, and in some cases flux. Here the predictions of key ETCs are: a) U. S. Regulatory Guide 1.99, Rev. 2 [20] ; b) EONY [17-19], which is in the alternate PTS Rule [21]: ASTM E900-15 [22]; c) JEAC 4201-13 Japan [23]; EdF 900 MW from France [24].

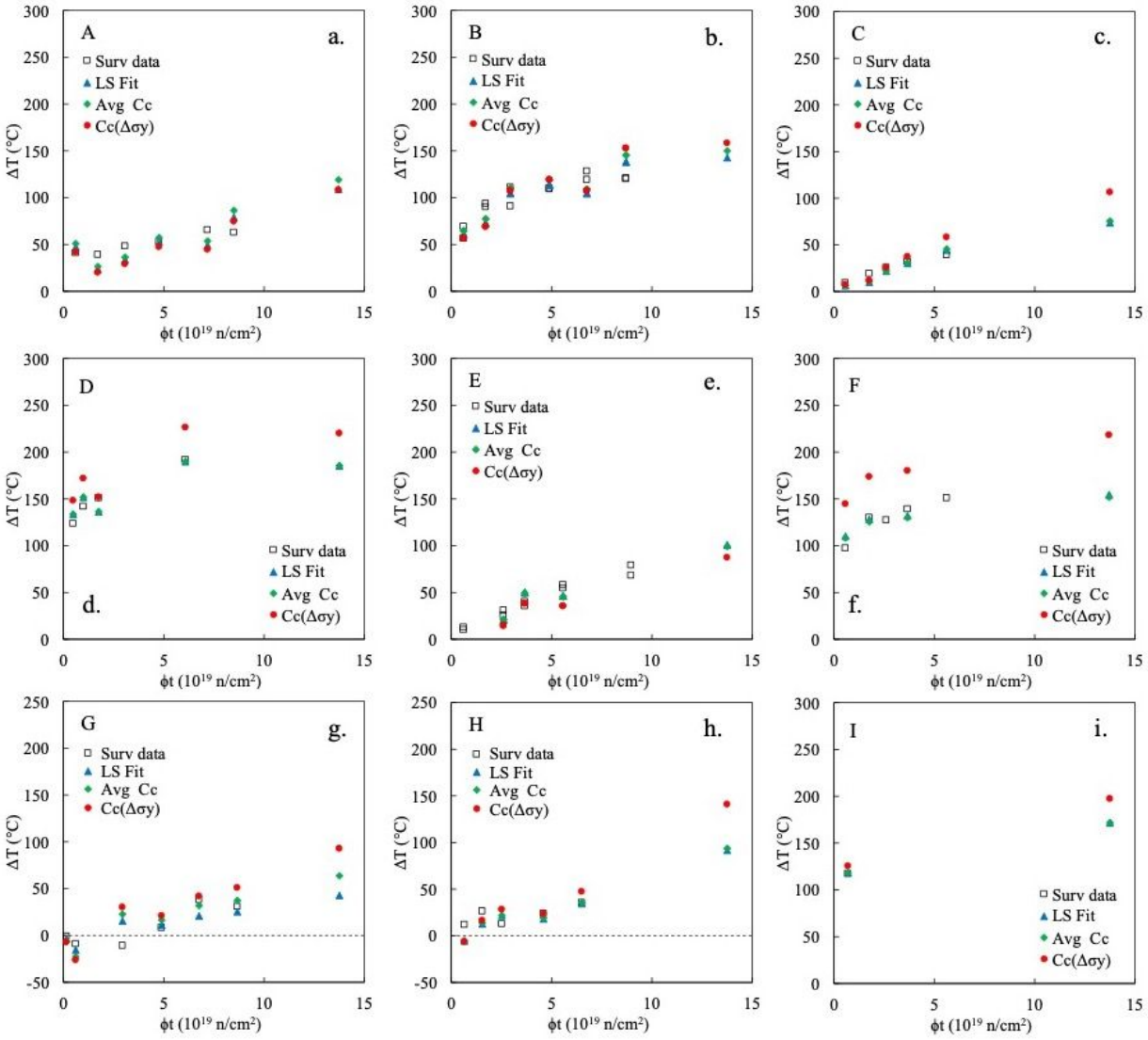


Figure 2a-i. Measured $\Delta T_c$ as a function of fluence for the surveillance data; the corresponding predicted $\Delta T_c$ estimates based on the tensile test $\Delta\sigma_y$ (in one case the average of the SPT and Hv converted $\Delta\sigma_y$) for the two individual steel and generic fit function $C_c$.

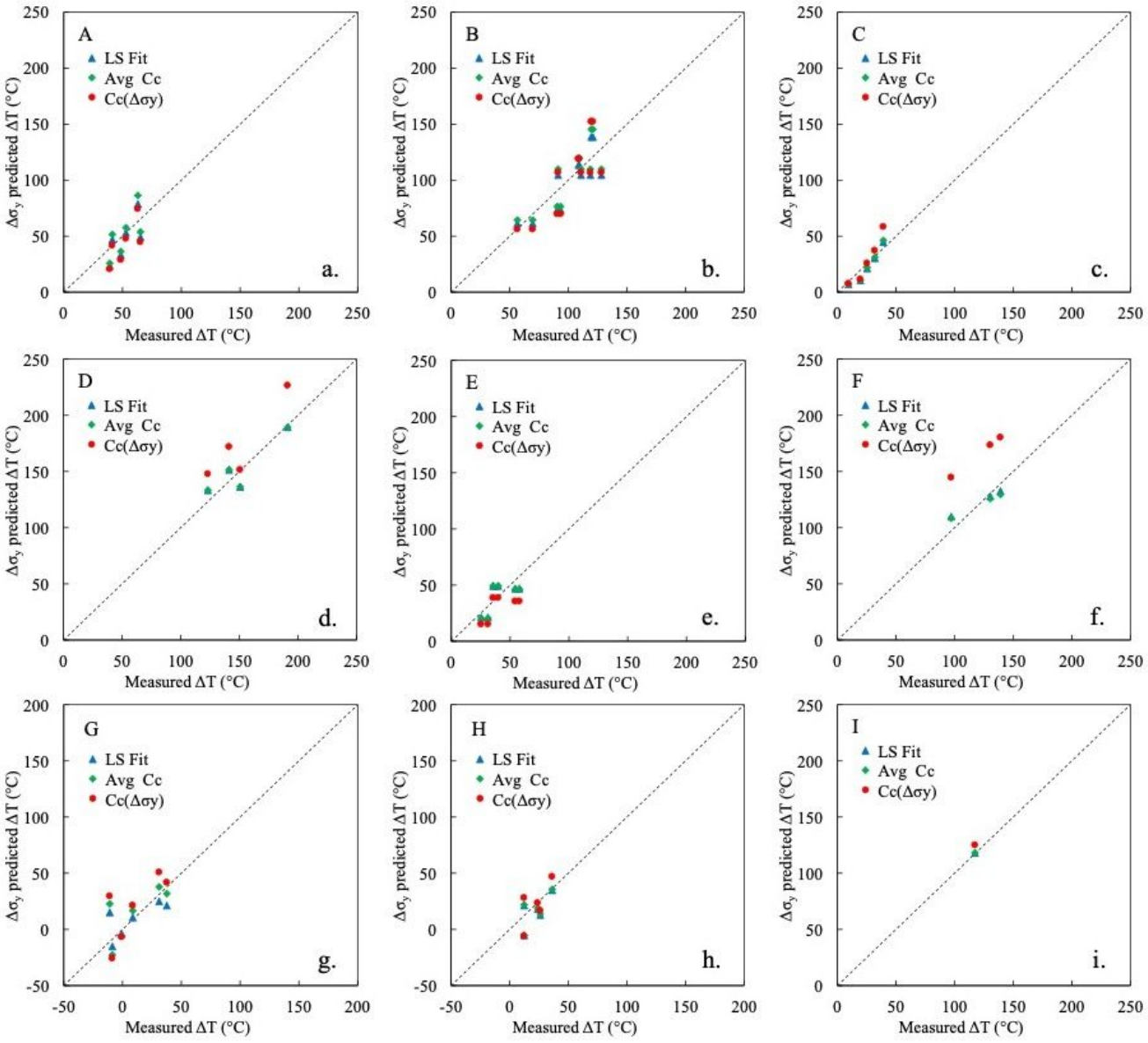


Figure 3a– i. Predicted versus measured $\Delta T_c$ for $C_c$'s least square fitted, averaged or from the generic fit.

Note, ASTM E900-15 is unique since it was developed by ASTM Committee E10.02 using surveillance capsule data (1878 data values) from thirteen countries and assessments of nine ETCs existing at the time [25]. Thus, ASTM E900-15 can be considered an *international* embrittlement trend equation. Countries that developed their own ETCs based on national surveillance capsule databases, rely on them to make embrittlement assessments and predictions

for their existing operating and possible new reactors. Since many countries seek to extend operating licenses for existing reactors to 80 years, or more, the choice of the most appropriate trend equation is very important, and requires reliable data reaching a fluence of about $10^{20}$ n/cm$^2$ for pressurized water reactors.

The prediction $\Delta T_C$ values from these five embrittlement prediction equations/methods are compared to the ATR-2 $\Delta T_C$ estimates as shown in Table 4. The predictions are based on the the mean of the fitted and averaged $C_c$, the chemistry content from Table 1 at 1.38 x $10^{20}$ n/cm$^2$ and 292˚C for the ATR-2 irradiation. On average the EDF FIS and JEAC 4201-13 overpredict the ATR-2 $\Delta T_c$ estimates, with a mean predicte minus measured bias of +28 and +15 ˚C and standard deviations of 21 and 50˚C, respectively. The EONY and E900 predictions underpredict the ATR-2 $\Delta T_c$ by -33 and -21, respectively, with standard deviations of 37 and 22 ˚C.

Table 4. Comparisons of ATR-2 $\Delta T_C$ estimates to predicted $\Delta T_C$ values from five embrittlement prediction equations/methods.

| Material Code | Tensile Yield to $\Delta T_c$, °C | $H_v$-SPT Average to $\Delta T_c$, °C | $\Delta T_c$ Predictions from Trend Equations, °C | | | | |
|---|---|---|---|---|---|---|---|
| | | | RG1.99, Rev. 2 | EONY | ASTM E900-15 | JEAC 4201 -13 | EDF 900 MW |
| A | 116 | 93 | 67 | 71 | 85 | 125 | 122 |
| B | 148 | 155 | 128 | 107 | 115 | 172 | 154 |
| C | 76 | 65 | 32 | 35 | 62 | 109 | 88 |
| D | NA* | 181 | 208 | 175 | 164 | 189** | 220** |
| E | 100 | 100 | 27 | 52 | 72 | 92 | 81 |
| F | 153 | 162 | 161 | 140 | 136 | 183 | 205 |
| G | 65 | 75 | 35 | 43 | 53 | 89 | 82 |
| H | 94 | 84 | 46 | 47 | 74 | 89 | 89 |

| | | | | | | | |
|---|---|---|---|---|---|---|---|
| I | 173 | 157 | 164 | 134 | 153 | 183 | 229 |
| Average Bias | | | -26 | -33 | -21 | 15 | 28 |
| Standard Deviation | | | 40 | 37 | 22 | 21 | 50 |

*No tensile data is available; **Assuming the maximum Cu = 0.3% for this Linde 92 weld [EONY].

## 4. The OWAY Model

The overriding objective of the ATR-2 experiment was to develop accurate predictions for predicting $\Delta T_c$ at low $\phi$, high $\phi t$ extended life conditions [2,6]. Special emphasis was also on the $\Delta\sigma_y$ contributions of Ni-Mn-Si precipitates, which are observed in a wide range of RPV steels at high $\phi t$. Unfortunately, there is little surveillance data in this fluence regime. Thus, the main goal of ATR-2 was to create and analyze the high fluence, intermediate flux database, for both $\Delta\sigma_y$ and microstructural changes, in a large matrix of irradiated alloys. The ATR-2 results were integrated with a variety of other databases to develop a new high $\phi t$-low $\phi$ predictive embrittlement procedure. The general approach of the so-called Odette, Wells, Almirall and Yamamoto (OWAY) model was based on four steps [2]:

1. Derive a composition dependent chemistry factor (CF = $\Delta\sigma_y$) for the ATR-2 condition just described.

2. Exploit the fact that neutron fluence dependence between intermediate ( ≈ 3-5x$10^{19}$

n/cm$^2$) and the high, extended life ATR-2 fluence (≈ 1.4x10$^{20}$ n/cm$^2$) is approximately linear.

3. Account for the flux difference between the ATR irradiation condition (≈ 3.68x10$^{12}$ n/cm$^2$-s) and low flux vessel service condition (≈ 4x10$^{10}$ n/cm$^2$-s) as an effective fluence, $\phi t_e$.

4. Interpolate between the intermediate and high effective fluence.

**Step 1**: The ATR-2 CF was based on 49 $\Delta\sigma_y$ data points and is given by:

$$CF = \Delta\sigma_y(\text{ATR-2}) = 127 + (Cu - Cu_{min})*570 + [(Cu - Cu_{min})*504 + 82.8](Ni - 0.75) + 20.7*(Mn+1.2Si)+1481*(1-3.73*(Cu - Cu_{min})*(P - P_{min}) \quad (1)$$

for $Cu_{min} = 0.04$, $Cu_{max} = 0.24$ and $P_{min} = 0.004$.

**Step 2**: The linear fluence dependence assumption is based on empirical observations of higher fluence surveillance data (surveillance reports, REAP, PLOTTER15, and the results for the 9 materials in this study), as well as some test reactor data [26-31], taken from the literature. Note an approximately linear fluence dependence is also supported by detailed physical models [2].

**Step 3**: The effect of flux was primarily determined by fitting a rate theory solute trap recombination model of $\phi t_e/\phi t < 1$ to high fluence $\Delta\sigma_y$ data over a range of higher test reactor fluxes to permit physically based extrapolation to low flux service conditions [2]. This analysis showed that the flux effect, which is strong at low fluence, decreases at high fluence ($\phi t_e$ -> $\phi t$), mainly due to the buildup of point defect sinks, suppressing defect recombination. The best effective fluence estimate was $\phi t_e \approx 1.25 \times 10^{20}$ n/cm$^2$, or ≈ 91% of the actual value of $\approx 1.4 \times 10^{20}$ n/cm$^2$ [2]. The corresponding practical bounds on $\phi t_e$ were estimated to be between ≈ 1 and $1.4 \times 10^{20}$ n/cm$^2$ (not considering uncertainness in the actual fluence estimates). The OWAY model was recently evaluated for 106 surveillance data points with $\phi t > 6 \times 10^{19}$ n/m$^2$ taken from the PLOTTER22 [32] database as will be described in full detail in a separate paper.

**Step 4**: Applying the OWAY model and interpolation to the 9 steels to predict high fluence $\Delta\sigma_y$ was carried out as follows:

- Evaluate $\Delta\sigma_y$ at low flux and intermediate fluence using either surveillance data above $3 \times 10^{19}$ and less than $5.5 \times 10^{19}$ n/cm$^2$, or based on ETC models such as E900 and EONY at $4 \times 10^{19}$ n/cm$^2$.
- Linearly interpolate between the intermediate fluence $\Delta\sigma_y$ and the ATR-2 chemistry factor

for effective fluences of 1 to 1.4x$10^{20}$ n/$cm^2$, including the best estimate $\phi t_e$ = 1.25x$10^{20}$ n/$cm^2$.

- Compare predictions of $\Delta\sigma_y$ at fluence greater than 5.5x$10^{19}$ n/cm2 for ATR-2 effective fluences of 1, 1.25 and 1.4x$10^{20}$ n/$cm^2$.

The results are shown in Figure 4. Here, the surveillance $\Delta T_c$ for the 9 steels was converted to $\Delta\sigma_y$ based on the individual steel $C_c$ values, as discussed above. The green circles are surveillances $\Delta\sigma_y$, unfilled diamonds are the ATR-2 CF, and filled diamonds are the measured ATR-2 data. Figures 4a-e use intermediate fluence surveillance data, which is available for 5 of the 9 steels. Figure 4f-i use EONY to predict the intermediate flux $\Delta\sigma_y$ at 4x$10^{19}$. A statisical analysis showed the best predictions were for a $\phi t_e \approx$ 1.4x$10^{20}$ (no flux effect). These results are consistent with an unpublished analysis of a larger data set.

Figure 5a shows the corresponding high fluence OWAY model predicted versus measured $\Delta\sigma_y$. Unfortunastely high fluence surveillance data was not available for 4 out of 9 alloys. Again, the OWAY model in Figure 5a, uses medium fluence surveillance data, when available. The standard deviation and average bias for OWAY are 13 and +3 MPa, respectively. Note the $\Delta\sigma_y$ for steel D are based on the EONY model at intermediate fluence, but are plotted in Figure 5a for

completeness. Further, there are two predicted $\Delta\sigma_y$ for steel D based on maximum Cu values of 0.24 and 0.3 wt.%, respectively, where the latter is pertinent to Linde 92 welds. Figure 5b-e show the other ETC predictions also have a small average bias, but somewhat larger standard deviations, than the OWAY $\Delta\sigma_y$. Table 4 tablulates the results in Figure 5.

Figure 6 shows predictions of the OWAY versus the other ETC models at $10^{20}$ n/cm$^2$. Again the EONY and E900 ETC models somewhat underpredict the OWAY $\Delta\sigma_y$, as does JAEC at high fluence. The FIS model overpredicts OWAY $\Delta\sigma_y$.

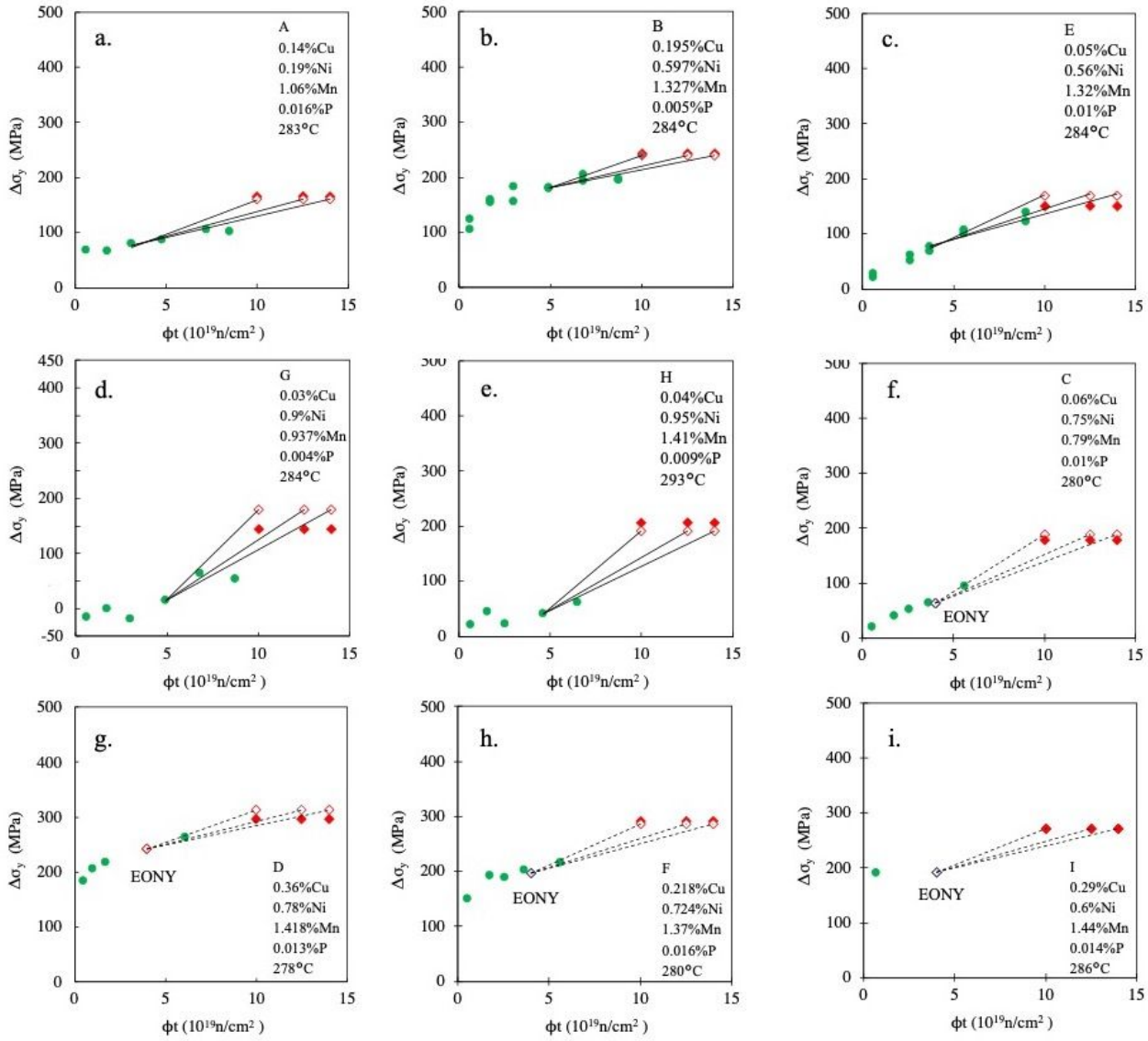


Figure 4. The OWAYmodel applied to the 9 steels: a-e) using intermediate fluence surveillance $\Delta\sigma_y$; f-i) EONY modeled intermediate fluence $\Delta\sigma_y$. The best predictions of higher fluence surveillance data are for an ATR-2 fluence ~ $14x10^{19}$ n/cm$^2$.

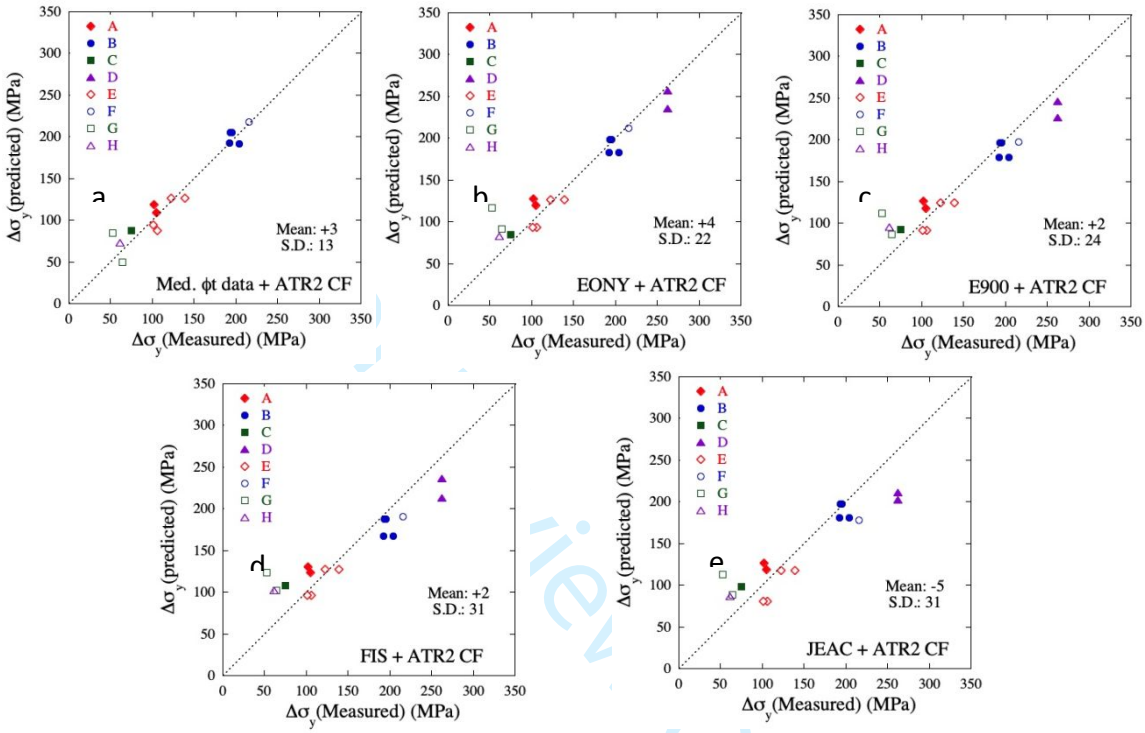


Figure 5. Measured versus predicted $\Delta\sigma_y$ for OWAY (5a) and other ETC models (5b-f).

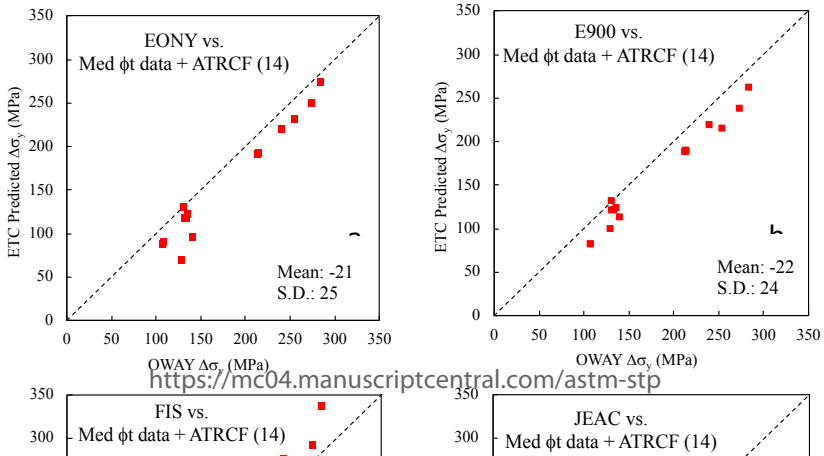

Figure 6. OWAY versus other ETC predictions at $1x10^{20}$ n/cm$^2$ and 290°C.

Table 5. OWAY and other ETC model predictions of high fluence surveillance $\Delta\sigma_y$.

| Steel | Measured $\Delta T_c$, °C | $\Delta\sigma_y$, MPa | $\Delta\sigma_y$ Predictions ($\phi t > \approx 5.5x10^{19}$) | | | | |
|---|---|---|---|---|---|---|---|
| | | | OWAY* | EONY | E900 | FIS | JEAC |
| A | 65 | 105 | 109 | 120 | 118 | 123 | 119 |
| A | 63 | 102 | 119 | 128 | 126 | 131 | 127 |
| B | 119 | 193 | 193 | 182 | 179 | 168 | 181 |
| B | 121 | 195 | 206 | 199 | 196 | 188 | 197 |
| B | 128 | 204 | 192 | 182 | 179 | 168 | 181 |
| B | 120 | 194 | 205 | 199 | 196 | 188 | 197 |
| C | 39 | 75 | 87 | 85 | 93 | 108 | 98 |
| D | 192 | 262 | *256* | 256 | 246 | 236 | 211 |
| D | 192 | 262 | *236* | 236 | 226 | 213 | 202 |
| E | 69 | 123 | 126 | 127 | 125 | 127 | 118 |

| | | | | | | | |
|---|---|---|---|---|---|---|---|
| E | 80 | 139 | 127 | 127 | 125 | 127 | 118 |
| E | 58 | 106 | 88 | 94 | 92 | 96 | 81 |
| E | 54 | 101 | 94 | 94 | 92 | 96 | 81 |
| F | 151 | 216 | 217 | 212 | 198 | 190 | 178 |
| G | 38 | 64 | 49 | 92 | 87 | 102 | 88 |
| G | 31 | 53 | 84 | 116 | 112 | 124 | 113 |
| H | 36 | 61 | 73 | 83 | 95 | 103 | 86 |

| | | | | | |
|---|---|---|---|---|---|
| Average bias | 2.6 | 4.5 | 1.8 | 1.9 | -4.6 |
| Standard deviation | 13 | 22 | 24 | 31 | 31 |



Table 6. Predictions of $\Delta\sigma_y$ at $1x10^{20}$ n/cm$^2$ and 290˚C.

| Steel | Predictions of $\Delta\sigma_y$ (MPa) at $10^{20}$ n/cm$^2$ and 290˚C | | | | |
|---|---|---|---|---|---|
| | OWAY14 | EONY | E900 | FIS | JEAC |
| A | 130 | 131 | 132 | 169 | 146 |
| A | 130 | 131 | 132 | 169 | 146 |
| A | 214 | 191 | 188 | 217 | 203 |
| B | 214 | 193 | 190 | 218 | 204 |

| | | | | | |
|---|---|---|---|---|---|
| B | 213 | 191 | 188 | 217 | 203 |
| B | 214 | 193 | 190 | 218 | 204 |
| B | 140 | 97 | 113 | 147 | 139 |
| C | *284* | 275 | 262 | 337 | 229 |
| D | *273* | 250 | 238 | 291 | 220 |
| D | 136 | 123 | 123 | 132 | 126 |
| E | 136 | 123 | 123 | 132 | 126 |
| E | 131 | 118 | 121 | 131 | 125 |
| E | 134 | 118 | 121 | 131 | 125 |
| E | 254 | 231 | 215 | 269 | 201 |
| F | 107 | 88 | 82 | 118 | 109 |
| G | 107 | 90 | 83 | 119 | 110 |
| G | 129 | 69 | 99 | 117 | 104 |
| H | *240* | 220 | 220 | 275 | 210 |
| I | | | | | |
| | Average bias | -21 | -22 | 11 | -16 |
| | Standard deviation | 25 | 24 | 20 | 26 |



## 5. Summary and Conclusions

The primary results and conclusions from this study of 9 archival surveillance steels irradiated in the ATR-2 experiment can be summarized as follows:

- The agreement between tensile, shear punch and microhardness test based estimates of changes in yield stress ($\Delta\sigma_y$) following the ATR-2 irradiation are generally good and well within data scatter.
- Published surveillance data on the $\Delta\sigma_y$ and 41 J Charpy shift ($\Delta T_c$) were analyzed to establish individual $\Delta T_c = C_c\Delta\sigma_y$ relations for the 9 steels.
- The predicted surveillance $\Delta T_c$ based on $\Delta\sigma_y$, using the individual steel $C_c$, are in good agreement with measured Charpy $\Delta T_c$.
- The predicted versus measured agreement of the $\Delta\sigma_y$ is much better than using a previously derived generic $C_c(\Delta\sigma_y)$ relation.
- To permit comparisons with predictions of various ETC models, the individual steel $C_c$ were used to predict $\Delta T_c$ at the ATR-2 condition based on the $\Delta\sigma_y$ from eight tensile and one shear punch plus microhardness test.
- On average the FIS and JAEC models slightly overpredict the ATR-2 $\Delta T_c$ condition estimates, while the EONY and E900 models result in underpredictions.

- The surveillance $\Delta T_c$ data was converted to $\Delta\sigma_y$ in order to test the OWAY model at high fluences greater than $5.5x10^{19}$ n/cm$^2$.
- The OWAY predictions are in excellent agreement with the high flunce surveillance data, assuming there is little or no effect of flux at the ATR-2 fluence, and that the $\Delta\sigma_y$ dependence is linear between intermediate ($\approx 4x10^{19}$n/cm$^2$) and the high ($\approx 1.4x10^{20}$ n/cm$^2$) fluences.
- The EONY, E900 and JAEC (at high fluence) ETC models underpredict the OWAY estimates of $\Delta\sigma_y$ at $10^{20}$ n/cm$^2$, while the Frensh FIS model slightly overpredicts the OWAY results.



## Acknowledgements

The co-authors wish to acknowledge and thank our recently departed lead author, Dr. Randy K. Nanstad, for his enumerable seminal contributions to nuclear reactor pressure vessel research. The large body of knowledge he created has supported the safe, long-term operation of nuclear power plants on an international basis. More generally, Randy's research also led to major improvemnts in our understanding of irradiation effects, fracture mechanics and structural materials. Bill Server acquired the nine surveillance steels studied in this paper under EPRI funding; and Randy authored a report on the technical findings under EPRI sponsorship. EPRI also partially supported the post-irradiation examinations of the nine steels. The UCSB ATR-2

irradiation was sponsored by the US DOE National Scientific Users Program, and was caried out as an UCSB-INL collaboration; we are very grateful for the outstanding ATR-2 INL team led by Dr. Mitch Meyer. Under the sponsorship of the US DOE Light Water Reacctor Sustainability Program, post irradiation characterization studies were mainly carried at UCSB by Drs. Peter Wellas and Nathan Almirall, with outstanding technical support from David Gragg. A wide variety of ORNL contributions contributed to the success of this research.

## References

1. T.J. Williams, R.K. Nanstad, "Low-Alloy Steels Low Alloy Steels," Ch 10, in G.R. Odette and S.J. Zinkle eds. *Structural Alloys for Nuclear Energy Applications*, Elsevier, 2019.
2. G.R. Odette, T. Yamamoto, T.J. Williams, R.K. Nanstad, C.A. English, "On the History and Status of Reactor Pressure Vessel Steel Ductile to Brittle Transition Temperature Shift Prediction Models," J. Nucl. Mater. 526 (2019) 151863.
3. N. Soneda, "Ch. 11 Embrittlement Correlation Methods to identify trends in embrittlement in reactor pressure vessels (RPVs)," (2014) 333-377 in *Irradiation Embrittlement of Reactor Pressure Vessels (RPVs)* in Nuclear Power Plants, first ed., Woodhead Publishing, 2014. doi:10.1533/9780857096470.3.333.
4. R.K. Nanstad, G.R. Odette, N. Almirall, J. Robertson, W.L. Server, T. Yamamoto, P. Wells, "Effects of ATR-2 Irradiation to High Fluence on Nine RPV Surveillance Materials," ORNL/TM-2017/172, Oak Ridge National Laboratory, December 2016
5. W.L. Server, T. C. Hardin, and N. A. Palm, 'U.S. Surveillance Programs for Long-Term Operation," *International Review of Nuclear Reactor Pressure Vessel Surveillance Programs, ASTM STP 1603*, W. L. Server and M. Brumovsky, Eds., ASTM International, West Conshohocken, PA, 2018, pp. 369-378
6. G.R. Odette, et. al, "Update on the High Fluence Advanced Test Reactor - 2 Reactor Pressure Vessel High Fluence Irradiation Project," UCSB ATR-2 2016-1, LWRS Report Number M3LW-16OR0402012, University of California, Santa Barbara, 30 June 2016.
7. As-Run Physics Analysis for the UCSB-2 Leadout Experiment in I-22, 2016.
8. As-Run Thermal Analysis of the UCSB-2 Experiment in the ATR, 2016.

9. H.B. Klasky, B.R. Bass, P.T. Williams, R.D. Phillips, M. Erickson, M.T. Kirk, G.L. Stevens, "Radiation embrittlement archive project," Trans SMiRT-22, August 18-23, 2013 San Francisco, CA.
10. M. Kirk, "User's Manual & ETC Assessment Guidelines – E10.02 PLOTTER Tool version 2013-10-04(R6)," 29 October , 2013 , ASTM International , West Conshohocken, PA .
11. *Standard Test Methods for Tension Testing of Metallic Materials*, ASTM E8/E8M-16ae1, (West Conshohocken, PA: ASTM International, approved August 1, 2016)
12. *Standard Test Method for Microindentation Hardness of Materials*, ASTM E384-16, (West Conshohocken, PA: ASTM International, approved February 1, 2016)
13. *Standard Test Methods for Vickers Hardness and Knoop Hardness of Metallic Materials,* ASTM E92-16, (West Conshohocken, PA: ASTM International, approved August 1, 2016)
14. T.S. Milot, "Establishing Correlations for Predicting Tensile Properties Based on the Shear Punch Test and Vickers Microhardness Data" [PhD Thesis], University of California, Santa Barbara, 2013
15. M.Y. He, G.R. Odette, T. Yamamoto, D. Klingensmith, "A universal relationship between indentation hardness and flow stress," J. Nuc. Mat. 367-370 (2007) 556.
16. D. Tabor, The hardness of solids, Rev. Phys. Tech 1 145 (1970).
17. G.R. Odette, P. Lombrozo, R. A. Wuellart, Relationship Between Irradiation Hardening and Embrittlement, Effect of Irradiation on Materials 12, ASTM STP 870 (1985) 840.

18. E.D. Eason, G.R. Odette, R.K. Nanstad, T. Yamamoto, "A physically based correlation of irradiation-induced transition temperature shifts for RPV steels," ORNL/TM-2006/530, Oak Ridge National Lab, (2007). (https://info.ornl.gov/sites/publications/files/Pub2592.pdf)
19. E.D. Eason, G.R. Odette, R.K. Nanstad, T. Yamamoto, A physically-based correlation of irradiation-induced transition temperature shifts for RPV steels, J. Nucl. Mater. 433 (2013) 240.
20. U.S. Nuclear Regulatory Commission, Radiation Embrittlement of Reactor Vessel Materials, Regulatory Guide 1.99 Rev. 2, 1988.
21. U.S. NRC, "10 CFR 50.61a Alternate fracture toughness requirements for protection against pressurized thermal shock events," March 24, 2021.
https://www.nrc.gov/reading-rm/doc-collections/cfr/part050/part050-0061a.html
22. Standard Guide for Predicting Radiation-Induced Transition Temperature Shift in Reactor Vessel Materials ASTM E900-21, (West Conshohocken, PA: ASTM International, approved September 23, 2021)
23. JEAC, Method of Surveillance Tests for Structural Materials of Nuclear Reactors, JEAC4201-2007 (2013 Addendum), Japan Electric Association, Chiyoda-ku, Tokyo, Japan, 2013.
24. P. Todeschini, Y. Lefebvre, H. Churier-Bossennec, N. Rupa, G. Chas and C. Benhamou, Revision of the irradiation embrittlement correlation used for the EDF RPV fleet, Proceedings of Fontevraud 7, (2010).

25. ASTM Subcommittee E10.02, Adjunct for ASTM E900-15: Technical Basis for the Equation used to Predict Radiation-Induced Transition Temperature shift in Reactor Vessel Materials," ASTM International, West Conshohocken, PA, 2015.

26. M. Shimodaira, T. Toyama, K. Yoshida, K. Inoue, N. Edbisawa, K. Tomura, T. Yoshiie, M.J. Konstantinovic, R. Gerard, Y. Nagai, "Contribution of irradiation-induced defects to hardening of a low-copper reactor pressure vessel steel," Acta Mater. 155 (15) (2018) pp. 402-409.

27. E.A. Kuleshova , B.A. Gurovich , Y.I. Shtrombakh , Yu.A. Nikolaev , V.A. Pechenkin , "Microstructural behavior of VVER-440 reactor pressure vessel steels under irradiation to neutron fluences beyond the design operation period," J. Nuc. Mat. 342 (2005) 77.

28. A. Ballesteros , I. Marcelles and J. Bros , "Beyond RPV design life," Nuclear Engineering International , 48 , 2003 , 32 .

29. M. Lambrecht, E. Meslin, L. Malerba, M. Hernandez, F. Bergner, B. Radiguet, A. Almazouzi, "On the correlation between irradiation-induced microstructural features and the hardening of reactor pressure vessel steels," Jou J. Nuc. Mat. 406-1 (2010) 84.

30. P. Efsing, J. Rouden, J, P. Nilsson, "Flux effects on radiation induced aging behavior of low alloys weld," Eff. Rad. Nuc. Mat. 26, ASTM-STP 1572 (2014) 119-134

31. L. Debarberis, F. Sevini, B. Acosta, A. Kryukov, D. Erak, "Fluence rate effects on irradiation embrittlement of model alloys," Int. J. Pres. Ves. Pip. 82 (2005) 373.

32. M. Kirk, PLOTTER 22 ASTM E10.02 Committee